Rotation Control of a 3-DOF Parallel Mechanism Driven by Pneumatic Muscle Actuators

LIU Kai*, *CHEN Yining*, *WU Yang*, *XU Jiaqi*, *WANG Yangwei*, *GE Zhishang*

College of Mechanical and Electrical Engineering, Nanjing University of Aeronautics and Astronautics, Nanjing 210016, P. R. China

Abstract: The pneumatic muscle actuator (PMA) has many advantages, such as good flexibility, high power / weight ratio, but its nonlinearity makes it difficult to build a static mathematical model with high precision. A new method is proposed to establish the model of PMA. The concept of hybrid elastic modulus which is related to the static characteristic of PMA is put forward, and the energy conservation law is used to achieve the expression of the hybrid elastic modulus, which can be fitted out based on experimental data, and the model of PMA can be derived from this expression. At the same time, a 3-DOF parallel mechanism (a new bionic shoulder joint) driven by five PMAs is designed. This bionic shoulder joint adopts the structure of two antagonistic PMAs actualizing a rotation control and three PMAs controlling another two rotations to get better rotation characteristics. The kinematic and dynamic characteristics of the mechanism are analyzed and a new static model of PMA is used to control it. Experimental results demonstrate the effectiveness of this new static model.

Key words: pneumatic muscle actuator; static mathematical model; hybrid elastic modulus; 3-DOF parallel mechanism

0 Introduction

Compared with traditional actuators, such as motor drivers and hydraulic drivers, the pneumatic muscle actuator (PMA) has the advantages of simple structure, good flexibility, convenient installation, low noise, high power / weight ratio and so on[1-4]. It has great potential for applications in bionic robot, mobility assistance[5] and can greatly improve the rehabilitative protocols for paraplegic patients[6]. Since the 1930s, many experts have done a lot of research on its structure design, characteristics of joints, control system and application, especially on the static characteristics. Chou and Hannaford[7] considered the elastic deformation and used the energy conservation law to achieve the static model of output force and pressure. Klute et al.[8] wrote a model including a non-linear Mooney-Rivlin mathematical description of the actuator's internal bladder. Kothera et al.[9] added the non-cylindrical tip shape and bladder thickness to improve the model that Ferraresi et al.[10] set up by the force balance method. The working process of PMA is nonlinear, that is, the input pressure is not proportional to the contraction force. It is difficult to establish an accurate theoretical model based on the energy conservation law or the force balance method, and there is a great gap between theoretical results and experimental results. Even considering factors such as the influence of PMA ends, rubber elastic force, and friction between fiber networks, the actual theoretical model is either very complex or still inconsistent with the actual model.

To get a comparatively simple and accurate static model of PMA, a quasi-static test platform is

---

designed and the concept of hybrid elastic modulus is proposed correspondingly. By combining the theoretical derivation with the experimental data, the model is established according to the material and structure characteristics of PMA and is compiled with the experimental data to obtain a completely new model of PMA, which can reflect its own characteristics and meet the precision requirements. In applications of PMA, it is common that two antagonistic PMAs were used to control a rotation joint[5,11-12]. Liu et al.[13] used four PMAs to control a 3-DOF parallel mechanism. At the same time, the PMA was widely used to drive the bionic arm[14-15]. In order to gain a bionic shoulder joint with better working characteristics, a new 3-DOF parallel mechanism controlled by five PMAs is designed. This mechanism has some advantages of the parallel mechanism and PMA together, such as the good flexibility and compact structure, and it also can be used to be a wrist joint or a neck joint[16].

In this paper, a new static model of PMA is firstly established by using the energy conservation law and the hybrid elastic modulus E which is fit out on the basis of experimental data. Then a 3-DOF parallel mechanism (a bionic shoulder joint) driven by five PMAs is designed. Finally, control experiments are done based on the new static model.

1   Static Characteristics of Pneumatic Muscle Actuator

PMA is composed of a rubber tube, a woven mesh, and two fixing components at the end. After the air is pumped in, the rubber tube will expand and pull the braid to make the artificial muscles produce the axial force. The geometric structure of PMA is illustrated in Fig.1. As shown from Fig.1

$$L = b\cos\theta \qquad (1)$$

$$D = \frac{b\sin\theta}{n\pi} \qquad (2)$$

where L is the length of PMA, D_i the inner diameter of the rubber tube, D the diameter of fiber layer, b the fiber length around the artificial muscle, n the number of turns, θ the angle between the fiber and the axis line of rubber tube and w the thickness of
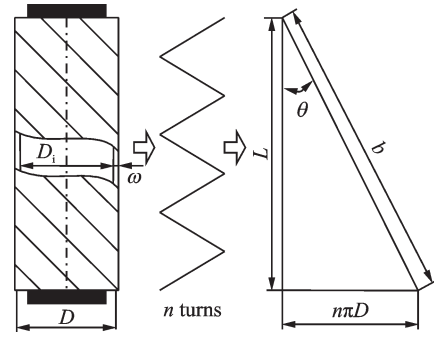
Fig.1   Geometric schematic of pneumatic artificial muscle

the rubber tube.

Assuming that the volume of the rubber tube is unchangeable in the process of contraction and relaxation, this can be described as

$$\pi D_0 L_0 w_0 = \pi D L w \qquad (3)$$

where D_0, L_0 and w_0 represent the initial diameter, the initial length and the initial thickness of PMA, respectively. Eqs.(1, 2) are brought into Eq.(3) to achieve the expression of the instantaneous thickness of rubber tube, which can be expressed as

$$w = w_0 \frac{\cos\theta_0\sin\theta_0}{\cos\theta\sin\theta} \qquad (4)$$

The hybrid elastic modulus E is set up to represent its overall elastic property, and it can be easily achieved by fitting the static test curves of PMA. Besides, the energy conservation law can be used to the contracting and expanding process of PMA. The energy change in the process of transition is expressed as

$$W_E + W_S = W_F + W_C \qquad (5)$$

where W_E is the energy that the fiber rubber tube have done in the axial direction, W_S the energy that the pressure have done in the radial direction, W_F the energy that external load have done and W_C the energy that the external pressure have done at two ends. Although the output force will change because of the nonlinearity of PMA, it can be regarded as a constant in small displacement.

Meanwhile, the hybrid elastic modulus E also can be considered as a constant in the tiny contraction. Eqs.(1)—(4) are brought into Eq.(5) to achieve the expression of W_E, W_S, W_F and W_C, which can be expressed as

$$W_{\mathrm{E}} = \int_{L_1}^{L_2} E \frac{L_0 - l}{L_0} \pi Dw\mathrm{d}l = \frac{Eb^2 w_1 \cos\theta_1 \sin\theta_1}{n} \left[\sqrt{2} \ (\cos\theta_1 - \cos\theta_2) + \ln\left(\frac{\cos\theta_2}{\cos\theta_1} \right) \right] \tag{6}$$

$$W_{\mathrm{s}} = \int_0^{L_2} \int_{r_1 - \frac{w_1}{2}}^{r_2 - \frac{w_2}{2}} 2\pi r p\mathrm{d}r\mathrm{d}l = \pi pb\cos\theta_2 \left[\left(\frac{b\sin\theta_2}{2\pi n} - \frac{w_0 \cos\theta_1 \sin\theta_1}{2\cos\theta_2 \sin\theta_2} \right)^2 - \left(\frac{b\sin\theta_1}{2\pi n} - \frac{w_1}{2} \right)^2 \right] \tag{7}$$

$$W_{\mathrm{F}} = \int_{L_1}^{L_2} F\mathrm{d}l = Fb(\cos\theta_2 - \cos\theta_1) \tag{8}$$

$$W_{\mathrm{C}} = \int_{L_1}^{L_2} \frac{\pi(D - w)^2}{4} p\mathrm{d}l = \frac{b^3 p}{4n^2 \pi} \left[\cos\theta_2 - \cos\theta_1 - \frac{1}{3} (\cos^3\theta_2 - \cos^3\theta_1) \right] - \frac{b^2 pw_1 \cos\theta_1 \sin\theta_1}{2n} \ln\left(\frac{\cos\theta_2}{\cos\theta_1} \right) +$$

$$\frac{\pi w_1^2 bp\cos^2\theta_1 \sin^2\theta_1}{4} \left[\frac{\cos\theta_1 - \cos\theta_2}{\cos\theta_1 \cos\theta_2} + \frac{1}{2} \ln \frac{(1 + \cos\theta_2)(1 - \cos\theta_1)}{(1 + \cos\theta_1)(1 - \cos\theta_2)} \right] \tag{9}$$

The quasi-static test platform uses FESTO's DMSP-10-100N-RM-CM PMA. The inner diameter is 10 mm, the initial length is 100 mm, the maximum allowable tension is 630 N, the maximum contraction percentage of the initial length is 25%, the initial braiding angle θ_0 is 45° and the outer diameter D_0 is 13.5 mm. In Fig.2, curves with the same color represent the two processes of the expansion and the contraction in the condition of the same pressure.

According to Eqs.(5)—(9), if the force F and other variables are known, the elastic modulus E will be calculated in the process of expansion as well as the process of contraction by the same way. As shown in Fig.3, six pictures severally describe the relationship between the elastic modulus E and the
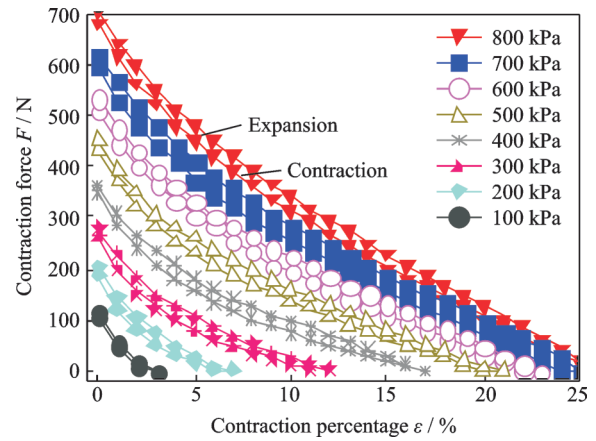
Fig.2   Static test curves of pneumatic artificial muscle

contraction percentage ε when the input pressure p is steady. The graphic relation is certainly clear and Eq.(10) is used to fit out the elastic modulus E.
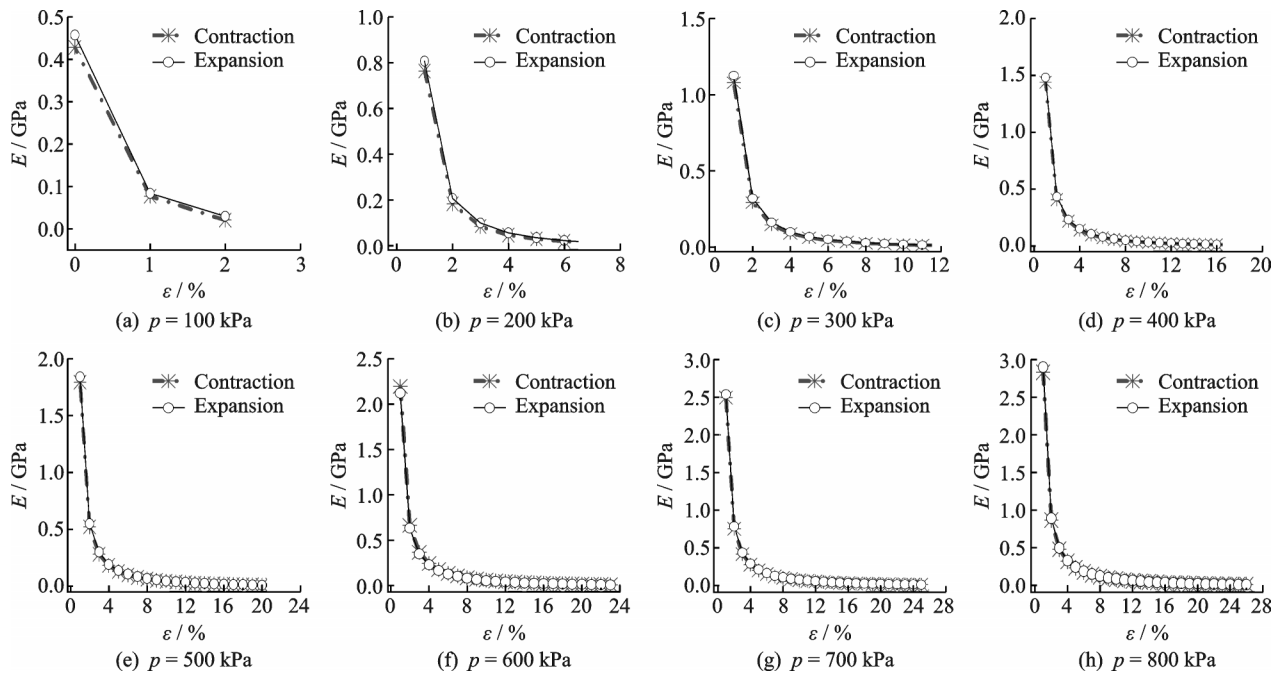
Fig.3   Relationship between elastic modulus ε and contraction percentage ε

The coefficients a, b, c and d are expressions related to the input pressure

$$E(p,\varepsilon)=a(p)/[1+b(p)\varepsilon+c(p)\varepsilon^2+d(p)\varepsilon^3]$$
(10)

Since Fig.3 shows the relationship between the hybrid elastic modulus and the contraction percent-age, values of the coefficients (a, b, c and d) can be achieved by the module of fitting linear curves in the origin software. Then, the relationship between the pressure and the coefficients is fitted to get the expressions of the coefficients $a(p)$, $b(p)$, $c(p)$ and $d(p)$, whose results are shown in Table 1.

Table 1   Fitting equations of coefficient and pressure in the process of contraction and expansion

Process of contraction		Process of expansion	
Predictive function	R-square	Predictive function	R-square
$a(p)=27.836\,32+3.511\,305\,91p$	0.99	$a(p)=67.592\,12+3.544\,570\,82p$	0.99
$b(p)=2.341\,28-0.000\,235\,92\,p$	0.97	$b(p)=2.223\,6-0.000\,100\,59p$	0.97
$c(p)=0.517\,28-0.000\,534\,01p$	0.90	$c(p)=0.427\,49-0.000\,424\,01p$	0.91
$d(p)=0.016\,69-0.000\,015\,87p$	0.96	$d(p)=0.018\,4-0.000\,018\,49p$	0.95

Since $a(p)$, $b(p)$, $c(p)$ and $d(p)$ have been expressed in Table 1, the expression of the elastic modulus E can be achieved by Eq.(10). Then, Eqs.(6)—(9) are brought into Eq.(5) to get an expression, which is the static model of PMA. For the convenience of the control, Eq.(5) and Eqs.(10)—(13) need to be integrated. Assuming that $A=W_E/E$, $B=W_S/E$, $C=W_F$, $D=W_C/p$, A, B, C and D are brought into Eq.(5) to get Eq.(11)

$$AE+Bp=C+Dp$$
(11)

Assuming that $a(p)=a_1+a_2p$, $b(p)=b_1+b_2p$, $c(p)=c_1+c_2p$, $d(p)=d_1+d_2p$, $a(p)$, $b(p)$, $c(p)$, $d(p)$ and Eq.(10) are brought into Eq.(11) to get Eq.(12)

$$K_1p^2+K_2p+K_3=0$$
(12)

where $K_1=(b_2\varepsilon+c_2\varepsilon^2+d_2\varepsilon^3)(B-D)$, $K_2=Aa_2+(1+b_1\varepsilon+c_1\varepsilon^2+d_1\varepsilon^3)(B-D)-(b_2\varepsilon+c_2\varepsilon^2+d_2\varepsilon^3)C$, $K_3=Aa_1-(1+b_1\varepsilon+c_1\varepsilon^2+d_1\varepsilon^3)C$. According to Eq.(12), if the force F and contraction percentage ε are known, the input pressure p will be figured out.

2   Design and Analysis of Parallel Mechanism

The structure design of the parallel experimental platform is shown in Fig.4. The large motion platform is connected to the fixed platform by three pneumatic muscle actuators (PMA1, PMA2 and PMA3), which make the large motion platform have two rotational degrees of freedom. Besides, the small motion platform is linked to the fixed plat-form by a spherical joint and is connected to the big motion platform by a revolute joint and two pneumatic muscle actuators (PMA4 and PMA5), which make the small motion platform have one rotational degree of freedom to the big motion platform.

2. 1   Kinematic analysis of parallel mechanism

The X-Y-Z Euler angle (α, β, γ) is taken to represent the posture of the small motion platform. The angle of coordinate system rotating around the O_1X_1 axis is γ; the angle of coordinate system rotating around the O_1Y_1 axis is β; and the angle of coordinate system rotating around the O_1Z_1 axis is α. So, ^1_2T, the transformation matrix from the moving coordinate system $O_2X_2Y_2Z_2$ to the fixed coordinate system $O_1X_1Y_1Z_1$, can be easily solved. Then the length L_{PMA1}, L_{PMA2}, L_{PMA3} of pneumatic muscle actuators (PMA1, PMA2, PMA3) can be expressed as

$$L_{PMA1}=\left|{}^1_2TP_{B_1}-P_{A_1}\right|,L_{PMA2}=\left|{}^1_2TP_{B_2}-P_{A_2}\right|$$
$$L_{PMA3}=\left|{}^1_2TP_{B_3}-P_{A_3}\right|$$
(13)

According to the moving coordinate system $O_2X_2Y_2Z_2$, the coordinate point B_4, B_5, C_1 and C_2 can be figured out. Then, the length of L_{PMA4} and L_{PMA5} are expressed as

$$L_{PMA4}=\left|P_{B_4}-P_{C_1}\right|,L_{PMA5}=\left|P_{B_5}-P_{C_2}\right|$$ (14)
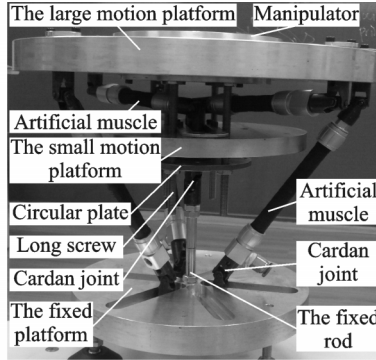
(a) Photograph of the 3-DOF parallel mechanism
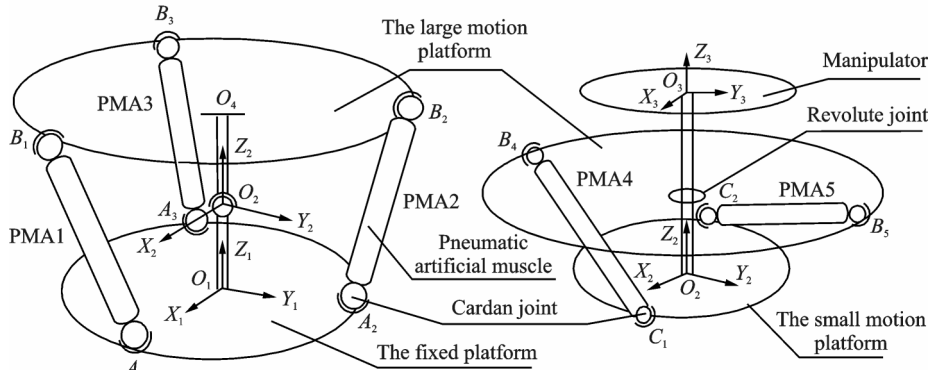
(b) Structure diagram of the 3-DOF parallel mechanism

Fig.4   Photograph and structure diagram of the 3-DOF parallel mechanism

2. 2   Dynamic analysis of parallel mechanism

Lagrange method is used to establish the dynamic equation of large motion platform[17]. The known Lagrange equation format is as follows.

$$L_E = K_E - P_E \tag{15}$$

where K_E is the kinetic energy, P_E the potential energy, and q the generalized coordinate vector of system. The following expression can be obtained.

$$\frac{\mathrm{d}}{\mathrm{d}t}\left(\frac{\partial L_E(q,\dot{q})}{\partial \dot{q}}\right) - \frac{\partial L_E(q,\dot{q})}{\partial q} = \tau \tag{16}$$

where τ denotes the generalized force (torque) vector acting on generalized coordinate. The roll, pitch, yaw (RPY) angle mentioned above is viewed as the generalized coordinate of the system, namely $q = [\gamma \ \beta \ \alpha]^T$. The following expression can be obtained by Eq.(16)

$$M(q)\ddot{q} + V(q,\dot{q}) + G(q) = \tau \tag{17}$$

where $M(q)$ denotes the inertia matrix of the system, $V(q,\dot{q})$ the Coriolis force and centrifugal force, and $G(q)$ the gravity. According to the principle of virtual work, the following equation can be obtained.

$$F = (J_1^T)^{-1} \cdot \tau =$$
$$(J_1^T)^{-1} \cdot [M(q)\ddot{q} + V(q,\dot{q}) + G(q)] \tag{18}$$

where F is the force vector composed of the output forces of PMA1, PMA2, PMA3, and J_1 is the Jacobian matrix of large motion platform.

Eq.(18) is the dynamic model of large motion platform. The derivation of the kinematic Eq.(13) can be obtained as

$$\dot{l} = J_1 \dot{q} \tag{19}$$

It is worth to point out that $V(q,\dot{q})$ has little or even no effect on the dynamics. Thus, Eq.(18) can be simplified as

$$F = (J_1^T)^{-1} \cdot \tau = (J_1^T)^{-1} \cdot [M(q)\ddot{q} + G(q)] \tag{20}$$

Because the small motion platform has only one rotational DOF around Z-axis, according to theorem of the rotating rigid body round fixed axis, the following equation can be obtained.

$$\tau_S = I_S \ddot{\theta} + c_S \dot{\theta} \tag{21}$$

where τ_S is torque needed to drive the small platform, I_S the moment of inertia of the small platform around Z-axis, and c_S the damping of the small platform.

On the other hand

$$\tau_s = 2F_s \times O_3C_1 \qquad (22)$$

Thus, according to Eqs.(21, 22), F_s can be calculated.

3 Control of Parallel Mechanism

As shown from the structure diagram of the test system (see Fig.5), the 3-DOF parallel mechanism is a system of multiple inputs and three outputs. Pneumatic pump provides servo valves with air pressure. According to the input analog signal (0—10 V), the control card (ART Technology, Xian, Shanxi, model number: PCI8201) controls the output pressure (0—0.8 MPa) of five servo valves by the channel 0—4. Five PMAs are severally connected to the corresponding servo valves by pipeline. Three rotational angles (α, β, γ) are measured by the gyroscope and fed back to the computer.

3.1 Rotation control of the large motion platform

The process of the closed‑loop control is shown in Fig.6, and it is a kind of feed‑forward control based on deviation. Two experiments of closed-loop control have been done (experiment 1: $\beta=0°$, $\gamma=0°——-10°$; experiment 2: $\gamma=0°$, $\beta=0°——-10°$), and the experimental results are shown as Figs.7 and 8. Besides, the maximum angle errors and average angle errors are calculated and shown in Table 2.

In Figs.7(a), 8(a), their average angle errors are $0.62°$ and $0.67°$ shown in Table 2, which indicates that the new mathematical model can be applied to this new parallel mechanism. But the change of pressure in closed-loop control has bigger oscillation due to the existence of compensations of the input pressure. According to Figs.7(b), 8(b), the bias pressure has some palpable jumps because of the large inertia when the mechanism starts to move.
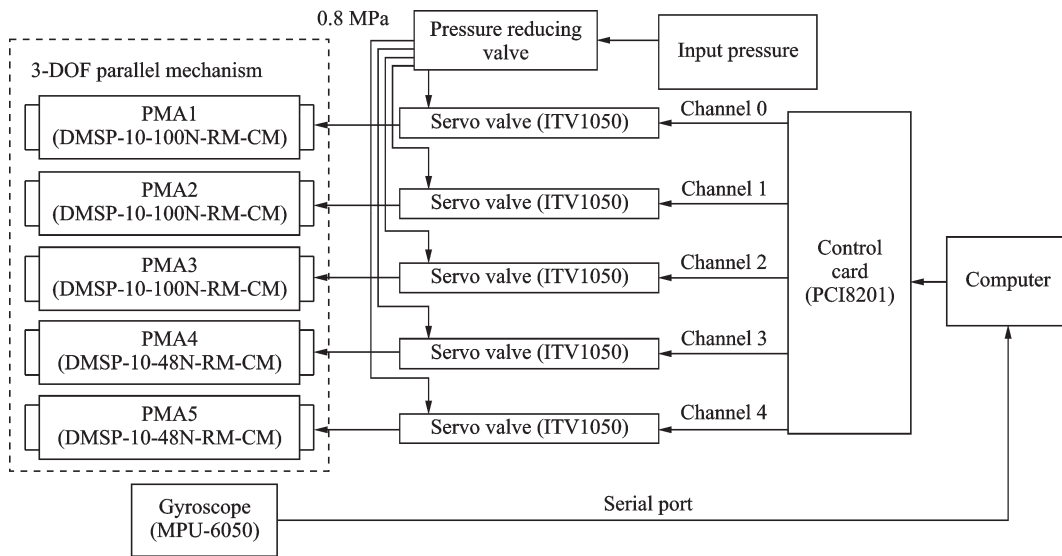
Fig.5 Block diagram of control system of 3-DOF parallel mechanism
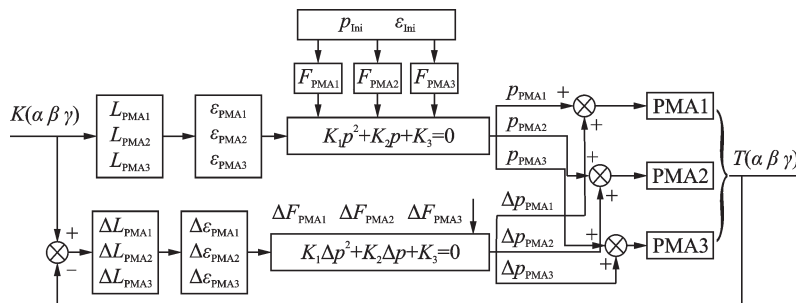
Fig.6 Block diagram of closed loop control of motion platform
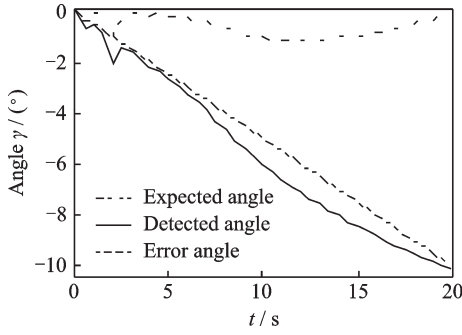
(a) Expected and detected angle γ of closed-loop control
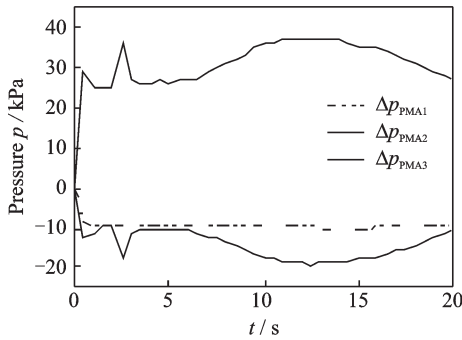
(b) Bias pressure in the process of γ from 0° to −10° (β=0°)

Fig.7 Error of the angle γ and change of the pressure in the process of γ from 0° to −10° (β=0°)
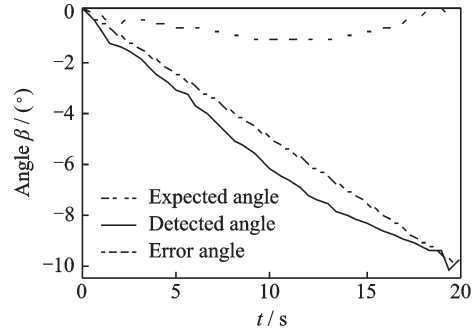
(a) Expected and detected angle β of closed-loop control
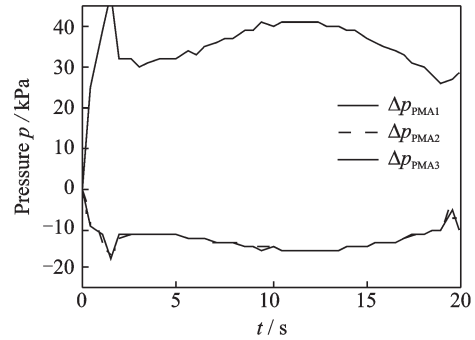
(b) Bias pressure in the process of β from 0° to −10° (γ=0°)

Fig.8 Error of the angle β and change of the pressure in the process of β from 0° to −10° (γ=0°)

Table 2 Comparison of rotational angle errors of the closed-loop control

Type of error	$\beta = 0°$, $\gamma = 0°$—$-10°$	$\beta = 0°$—$-10°$, $\gamma = 0°$	$\alpha = 39°$—$89°$
Maximum angle error	1.15	1.18	1.95
Average angle error	0.62	0.67	1.02

3.2 Rotation control of the manipulator

In the feed-forward, the contraction percentage ε_{PMA4} and ε_{PMA5} can be figured out by the target rotation angle θ_d in Fig.9. According to the contraction percentage (ε_{PMA4} and ε_{PMA5}) and the given contraction force (F_{PMA5}, F_{PMA6}), the instantaneous pressure (p_{PMA4}, p_{PMA5}) can be obtained and then applied to two pneumatic muscle actuators (PMA4 and PMA5).

For the convenience of control, set $F_{PMA4}=F_{PMA5}=58$ N and $\Delta F_{PMA4}=\Delta F_{PMA5}=\Delta F=30$ N during the test. The curves of closed loop-control are shown in Fig.10. Besides, the maximum angle error and average angle error are calculated and shown in Table 2.

In Fig.10(a), the maximum angle error of closed-loop control calculated is 1.95°, and the average angle error is 1.02°. Both the maximum angle error and the average angle error are bigger than that of the large motion platform because the rotation angle of the manipulate changes from 39° to 89°, which is bigger than the rotation angle of the large motion platform. And, the tracking accuracy of the closed-loop control has great accuracy.
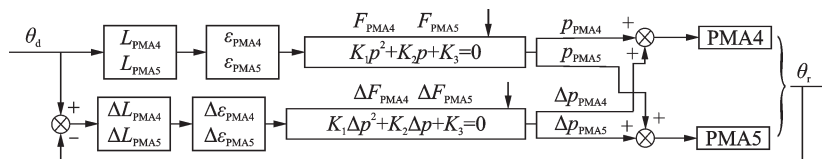
Fig.9 Block diagram of closed-loop control of the manipulator

(a) Expected and detected angle α of closed-loop control

(b) Bias pressure of PMA4 and PMA5
in the process of α from 39° to 89°
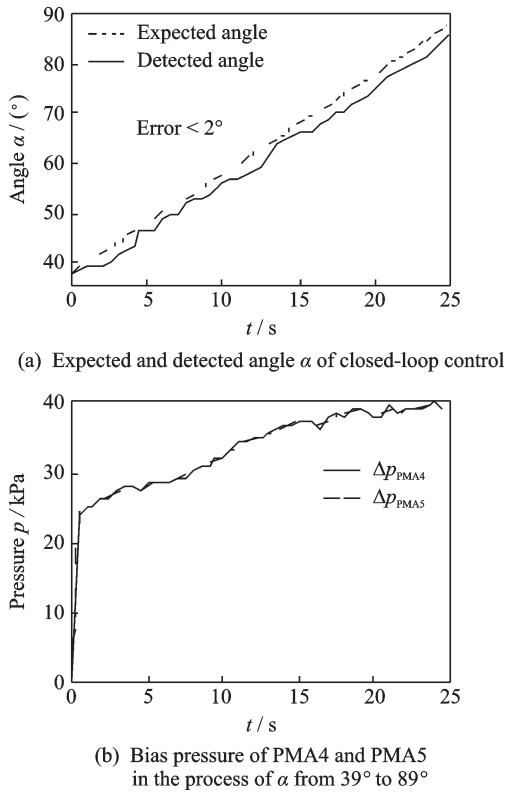
Fig.10　Error of the angle α and change of the pressure in the process of α from 39° to 89°

4　Conclusions

This article puts forward a new idea of establishing the static model of PMA, assuming that the energy is conserved in the instantaneous expanding or contracting process of PMA, and derives the quantitative value of the elastic modulus in the process of the shrinking or stretching of PMA. Then hybrid elastic modulus is fitted out to predict the relationship between contraction force, contraction percentage and the input pressure. Besides, the hybrid elastic modulus E is set up to avoid considering multiple nonlinear factors separately and simplifies the process of building this new model.

To validate the control accuracy of the new static model, a special parallel mechanism driven by five PMAs is designed. This parallel mechanism with three rotational degrees of freedom can be used as bionic shoulder joint and has advantages of good flexibility, no pollution, low cost, high power / weight ratio and so on. Afterwards, the inverse kinematics of this parallel mechanism is analyzed, and the parallel mechanism by using this new static

mathematical model is effectively controlled. According to many experiments, the average angle error is almost $0.6°$ in the closed-loop control system, which verifies the effectiveness of this static model.

References

[1]　SERRES J L, REYNOLDS D B, PHILLIPS C A, et al. Characterisation of a phenomenological model for commercial pneumatic muscle actuators[J]. Computer Methods in Biomechanics & Biomedical Engineering, 2009, 12(4): 423-430.

[2]　CHANG M K. An adaptive self-organizing fuzzy sliding mode controller for a 2-DOF rehabilitation robot actuated by pneumatic muscle actuators[J]. Control Engineering Practice, 2010, 18(1): 13-22.

[3]　HOSOVSKY A, HAVRAN M. Dynamic modeling of one degree of freedom pneumatic muscle-based actuator for industrial applications[J]. Tehnicki Vjesnik, 2012, 19(3): 673-681.

[4]　LIU K, GE Z S, XU J Q, et al. Kinematic optimization of bionic shoulder driven by pneumatic muscle actuators based on particle swarm optimization[J]. Transactions of Nanjing University of Aeronautics and Astronautics, 2016, 33(3): 301-309.

[5]　CHOI T Y, CHOI B S, SEO K H. Position and compliance control of a pneumatic muscle actuated manipulator for enhanced safety[J]. IEEE Transactions on Control Systems Technology, 2011, 19(4): 832-842.

[6]　HASSANI W, MOHAMMED S, RIFAI H, et al. Powered orthosis for lower limb movements assistance and rehabilitation[J]. Control Engineering Practice, 2014, 26(3): 245-253.

[7]　CHOU C P, HANNAFORD B. Measurement and modeling of McKibben pneumatic artificial muscles [J]. IEEE Transactions on Robotics and Automation, 1996, 12(1): 90-102.

[8]　KLUTE G K, HANNAFORD B. Accounting for elastic energy storage in McKibben artificial muscle actuators[J]. Journal of Dynamic Systems Measurement & Control, 2000, 122(2): 386-388.

[9]　KOTHERA C S, JANGID M, SIROHI J, et al. Experimental characterization and static modeling of McKibben actuators[J]. Journal of Mechanical Design, 2009, 131(9): 357-367.

[10]　FERRARESI C, FRANCO W, MANUELLO B A. Flexible pneumatic actuators: A comparison between the McKibben and the straight fibres muscle[J]. Journal of Robotics and Mechatronics, 2001, 13(1): 56-63.

[11] VOCKE R D, KOTHERA C S, WERELEY N M. Mechanism and bias considerations for design of a bi-directional pneumatic artificial muscle actuator[J]. Smart Materials & Structures, 2014, 23(12): 407-414.

[12] YU H T, GUO W, TAN H W, et al. Design and control on antagonistic bionic joint driven by pneumatic muscles actuators[J]. Journal of Mechanical Engineering, 2012, 48(17): 1-9. (in Chinese)

[13] LIU Y, WANG T, FAN W, et al. Model-free adaptive control for the ball-joint robot driven by PMA group[J]. Robot, 2013, 35(2): 129-134. (in Chinese)

[14] ANH H P H, AHN K K. Hybrid control of a pneumatic artificial muscle (PAM) robot arm using an inverse NARX fuzzy model[J]. Engineering Applications of Artificial Intelligence, 2011, 24(4): 697-716.

[15] XU Z, KUMAR V, TODOROV E. A low-cost and modular, 20-DOF anthropomorphic robotic hand: Design, actuation and modeling[C]//The 13th IEEE-RAS International Conference on Humanoid Robots. Atlanta: IEEE, 2015: 368-375.

[16] LIU K, XU J Q, GE Z S, et al. Robust control of 3-DOF parallel robot driven by PMAs based on nominal stiffness model[J]. Advanced Robotics, 2017, 31(10): 531-543.

[17] CHEN B, XIE B, DING L, et al. Dynamical model identification for industrial robot with payload[J]. Journal of Nanjing University of Aeronautics & Astronautics, 2016, 48(6): 835-841. (in Chinese)

Authors   Dr. **LIU Kai** is an associate professor at College of Mechanical and Electrical Engineering, Nanjing University of Aeronautics and Astronautics (NUAA), China. He received his Ph.D. degree from NUAA in 2007. His main research interest is bionic robot and numerical control technology.

Ms. **CHEN Yining** received her B.S. degree from NUAA, in 2017. She is currently pursuing master degree in NUAA. Her research interests are primarily in the area of pneumatic muscle actuator and robotics.

Mr. **WU Yang** received his B.S. degree from Nanjing Agricultural University, China, in 2016. He is currently pursuing master degree in NUAA. His research interests are primarily in the area of motion control and bionic robot.

Mr. **XU Jiaqi** received his B.S. degree from Nanhang Jincheng College, China, in 2015. He is currently pursuing master degree in NUAA. His research interests are primarily in the area of motion control and robotics.

Dr. **WANG Yangwei** received his M.S. and Ph.D. degrees from Harbin Institute of Technology (HIT), China. He is currently a lecturer at the College of Mechanical and Electrical Engineering of NUAA in Nanjing, China. His research interests include bionic robot, robotics and control system.

Mr. **GE Zhishang** received his M.S. degree from NUAA in 2017. His research interests are primarily in the area of motion control and measurement system.

Author contributions   Dr. **LIU Kai** was in charge of the whole trial. Ms. **CHEN Yining** analyzed the results and wrote the manuscript. Mr. **WU Yang** designed the platforms and assisted with sampling. Mr. **XU Jiaqi** and Mr. **GE Zhishang** assisted with the laboratory analyses and modeling. Dr. **WANG Yangwei** contributed to the background of the study. All authors commented on the manuscript draft and approved the submission.

Competing interests   The authors declare no competing interests.

(Production Editor: Wang Jing)